Magnetic discrimination between Al-substituted hematites synthesized by hydrothermal and thermal dehydration methods and its geological significance

Zhaoxia Jiang,[1,2] Qingsong Liu,[1] Vidal Barrón,[3] José Torrent,[3] and Yongjae Yu[4]

Received 22 June 2011; revised 20 December 2011; accepted 24 December 2011; published 23 February 2012.

[1] Hematite, a ubiquitous mineral in aerobic sediments and soils of temperate and warm areas, is weakly magnetic. However, it carries a stable natural remanent magnetization, and thus can reflect paleoenvironment changes. To quantify the influence of Al content in hematite on its magnetic properties, two series of hematite particles were prepared by hydrothermal transformation of ferrihydrite in aqueous suspension (HFh* series) and by thermal dehydration of goethite (HG* series). Crystal morphological and mineral magnetic properties of these two types of hematites differ distinctively. More specifically, the HFh* series samples display oblate (plate-like) morphologies, while the HG* series samples are prolate (highly acicular). HFh* series samples display higher saturation magnetization but lower magnetic coercivity than that of the HG* series. It is tenable that a better lattice ordering of Al substitution occurs during the process of dehydration of goethite than after transformation from ferrihydrite, resulting in weaker saturation magnetization for HG* series samples. The origin of single domain (SD) hematite in nature can be diagnosed by the correlation of unblocking temperature and magnetic coercivity: a positive correlation indicates the presence of pure (Al-free) SD hematite, while a negative correlation indicates a chemical origin of SD Al-substituted hematite. These results bear new information on decoding the complex magnetic properties of SD Al-hematite in nature environments, and thus deepen our understanding of the mechanism of variations in both paleomagnetic and paleoenvironmental signals carried by Al-hematite.

Citation: Jiang, Z., Q. Liu, V. Barrón, J. Torrent, and Y. Yu (2012), Magnetic discrimination between Al-substituted hematites synthesized by hydrothermal and thermal dehydration methods and its geological significance, *J. Geophys. Res.*, *117*, B02102, doi:10.1029/2011JB008605.

1. Introduction

[2] Hematite (α-Fe_2O_3) occurs in significant proportion in many aerobic soils under warm and humid climates or in sediments of various ages [*Walker*, 1967a; *Walker et al.*, 1981; *Christensen et al.*, 2000]. Although hematite is weakly magnetic compared to other iron (Fe) oxides (e.g., the ferrimagnetic magnetite and titanomagnetite), its contribution to the magnetic anomaly cannot be ignored. In fact, hematite is the dominant magnetic carrier in many lithologic units [*Walker*, 1967b]. Moreover, the formation and preservation of hematite is sensitive to the surrounding environment. Therefore, mineral magnetic characterizations of hematite can be used as paleoenvironmental proxies.

[3] In natural environments, there are two dominant pathways for the formation of hematite. One is the hydrothermal transformation of ferrihydrite, either in soils [*Cornell and Schwertmann*, 2003] or aerobic sedimentary environments [*Spencer and Percival*, 1952; *Drodt et al.*, 1997; *Eren and Kadir*, 1999; *van der Zee et al.*, 2003]. Thus, the precipitation of ultra-fine-grained hematite from iron-rich solutions in the pore spaces of clastic sediments results in the distinctive purple to red hues of the red beds [*Walker*, 1967a; *Dunlop and Özdemir*, 1997]. In the deep sea, hematite is observed only above the redox boundary, serving as an indicator of oxidizing conditions. Its abundance decreases with a linear gradient from about 20 wt% of the total Fe-oxide close to the sediment surface to about zero at the redox boundary, resulting in the color change of the sediment around the redox boundary from red to green [*Drodt et al.*, 1997; *Eren and Kadir*, 1999]. On the surface of Mars, most hematite is possibly formed from Fe-rich aqueous fluids under ambient conditions or hydrothermal fluids. It has been proposed that the presence of crystalline

[1]State Key Laboratory of Lithospheric Evolution, Institute of Geology and Geophysics, Chinese Academy of Sciences, Beijing, China.
[2]Graduate School of the Chinese Academy of Sciences, Beijing, China.
[3]Departamento de Agronomía, Universidad de Córdoba, Córdoba, Spain.
[4]Department of Geology and Earth Environmental Sciences, Chungnam National University, Daejeon, South Korea.

0148-0227/12/2011JB008605

Table 1. Methods Used to Synthesize the Hematite Samples

Sample	Starting Reagents/Products	Aging Temperature (°C)	Time
HFh0	100 mL 0.4 M $Fe(NO_3)_3$ + 1 M NaOH to pH = 9 and L-tartrate 0.0008 M	95	21 days
HFh2	100 mL 0.392 M $Fe(NO_3)_3$ + 0.008 M $Al(NO_3)_3$ + 1 M NaOH to pH = 9 and L-tartrate 0.0008 M	95	21 days
HFh4	100 mL 0.384 M $Fe(NO_3)_3$ + 0.016 M $Al(NO_3)_3$ + 1 M NaOH to pH = 9 and L-tartrate 0.0008 M	95	21 days
HFh8	100 mL 0.368 M $Fe(NO_3)_3$ + 0.032 M $Al(NO_3)_3$ + 1 M NaOH to pH = 9 and L-tartrate 0.0008 M	95	21 days
HFh16	100 mL 0.336 M $Fe(NO_3)_3$ + 0.064 M $Al(NO_3)_3$ + 1 M NaOH to pH = 9 and L-tartrate 0.0008 M	95	21 days
HGH0	Goethite prepared with 100 mL 0.6 M $Fe(NO_3)_3$+ 100 mL 5 M NaOH aged at 60 °C	800	4 h
HGH2	Goethite prepared with 100 mL 0.588 M $Fe(NO_3)_3$ + 0.012 M $Al(NO_3)_3$ + 100 mL 5 M NaOH aged at 60 °C	800	4 h
HGH4	Goethite prepared with 100 mL 0.576 M $Fe(NO_3)_3$ + 0.024 M $Al(NO_3)_3$ + 100 mL 5 M NaOH aged at 60 °C	800	4 h
HGH8	Goethite prepared with 100 mL 0.552 M $Fe(NO_3)_3$ + 0.048 M $Al(NO_3)_3$ + 100 mL 5 M NaOH aged at 60 °C	800	4 h
HGH16	Goethite prepared with 100 mL 0.504 M $Fe(NO_3)_3$ + 0.096 M $Al(NO_3)_3$ + 100 mL 5 M NaOH aged at 60 °C	800	4 h
HGH20	Goethite prepared with 100 mL 0.48 M $Fe(NO_3)_3$+ 0.12 M $Al(NO_3)_3$ + 100 mL 5 M NaOH aged at 60 °C	800	4 h
HGH30	Goethite prepared with 100 mL 0.42 M $Fe(NO_3)_3$+ 0.18 M $Al(NO_3)_3$ + 100 mL 5 M NaOH aged at 60 °C	800	4 h
HGL0	Goethite prepared oxidizing 1 L 0.05 M $FeSO_4$ + 110 mL 1 M $NaHCO_3$	800	4 h
HGL4	Goethite prepared oxidizing 1 L 0.048 M $FeSO_4$ + 0.002 M $Al(NO_3)_3$ +110 mL 1 M $NaHCO_3$	800	4 h
HGL8	Goethite prepared oxidizing 1 L 0.046 M $FeSO_4$ + 0.004 M $Al(NO_3)_3$ +110 mL 1 M $NaHCO_3$	800	4 h
HGL16	Goethite prepared oxidizing 1 L 0.042 M $FeSO_4$ + 0.008 M $Al(NO_3)_3$ +110 mL 1 M $NaHCO_3$	800	4 h
HGL20	Goethite prepared oxidizing 1 L 0.04 M $FeSO_4$ + 0.01 M $Al(NO_3)_3$ +110 mL 1 M $NaHCO_3$	800	4 h
HGL30	Goethite prepared oxidizing 1 L 0.035 M $FeSO_4$ + 0.015 M $Al(NO_3)_3$ +110 mL 1 M $NaHCO_3$	800	4 h

hematite mineralization on Mars can be used as an evidence for the presence of near surface water [*Christensen et al.*, 2000, 2001].

[4] The other pathway for the formation of hematite is thermal dehydration of a precursor Fe oxyhydroxide (e.g., $2FeOOH \rightarrow Fe_2O_3 + H_2O$), which is considered to be the main origin of hematite in igneous and sedimentary rocks [*de Boer et al.*, 2001]. In particular, the acicular hematite formed from the dehydroxylation of goethite has received much attention, given that goethite is the most widespread Fe oxide (a term used here to encompass oxides, hydroxides and oxyhydroxides) in soils and sediments [*Cornell and Schwertmann*, 2003]. Once a soil experiences an intense forest fire or enters in contact with a hot lava flow, goethite is transformed into hematite [*Iglesias et al.*, 1997; *Ketterings et al.*, 2000; *Nørnberg et al.*, 2009]. *Rendón et al.* [1983] found this transformation to be complete at >600°C after studying the systematic transformation from goethite to hematite. *Diakonov et al.* [1994] investigated the thermodynamic properties of goethite synthesized in aqueous solutions and hematite obtained from the dehydroxylation of goethite and found a relationship between the surface area and the heat capacity or entropy of goethite.

[5] The hematite samples used in this study were synthesized via (1) hydrothermal transformation of ferrihydrite in aqueous suspension for several days, and (2) thermal dehydroxylation of goethite prepared by aging ferrihydrite suspensions at high pH. The morphological, crystallochemical and magnetic properties of these different hematite particles were characterized and the paleomagnetic and paleoenvironmental significances of these properties were investigated.

2. Samples and Experiments

[6] The synthesis procedures for the samples are summarized in Table 1. The samples of the HFh* series (HFh0, HFh2, HFh4, HFh8, HFh16, where HFh and the following number represent hematite transformed from ferrihydrite and the initial mol% Al [i.e., the molar Al/(Fe + Al) ratio expressed in percentage], respectively), were prepared by mixing 100 ml of 0.4 M (Fe, Al) $(NO_3)_3$ with 1 M sodium hydroxide (NaOH) to a final pH of 9 [*Barrón et al.*, 1984]. After precipitation, in order to prevent the formation of goethite [*Cornell and Schwertmann*, 1979], L-tartrate in a concentration of 8×10^{-4} M was immediately added and then the suspension of ferrihydrite was aged at 95°C in an oven. For the samples of the HG* series, the primary reagent was goethite which was obtained either by aging a Fe(III) salt in 5 M NaOH at 60°C (subseries HGH*) or prepared with precipitation and oxidation of a Fe (II) salt at room temperature (subseries HGL*) [*Torrent et al.*, 1990; *Schwertmann and Cornell*, 2000]. A total of 13 samples were prepared (HGH0, HGH2, HGH4, HGH8, HGH16, HGH20, HGH30, HGL0, HGL4, HGL8, HGL16, HGL20 and HGL30, where HG stands for hematite transformed from thermal dehydration of goethite, while H and L following HG represent the high and low crystallinity, respectively, and the number represents the initial mol% Al).

[7] The synthesized products were washed free of salts by centrifuging the suspension, discarding the supernatant, and resuspending and dialyzing the sediment in deionized water until the electrical conductivity of the equilibrium solution became <0.01 dS/m. Finally, the suspension was dried at 60°C. Then, HG* series hematites were obtained by heating the precursor HG* goethites at 800°C for 4 h.

[8] The authentic mol% of Al incorporated in the solid phase was determined by atomic absorption spectrometry (AAS) after dissolving the samples in concentrated HCl. Powder X-ray diffraction (XRD) patterns were obtained with a Siemens D5000 diffractometer with monochromatized Co$K\alpha$ radiation, a step size of 0.05° 2θ, and a counting time of 20 s. For quantitative morphological analysis, the width of half-height (WHH) is inversely proportional to the mean crystal thickness perpendicular to a given *hkl* plane (provided that the crystal diffracts coherently). The (104) and (110) planes correspond to a nearly basal plane (i.e., one that is nearly perpendicular to the *c* crystallographic axis) and a plane that is parallel to the *c* axis, respectively. Hence, the WHH was estimated for (104) and (110) lines from the XRD data, denoted as WHH(104) and WHH(110), respectively. In

addition, WHH(104) and WHH(110) represent approximate crystal thickness normal to the basal (104) and prismatic (110) planes, respectively. Then, the WHH(104)/WHH(110) ratio provides an estimate of the diameter/thickness (in the *c* direction) of the hematite particles [*Schwertmann et al.*, 1979; *Barrón et al.*, 1984; *Schwertmann and Cornell*, 2000].

[9] Transmission electron micrographs (TEM) were obtained with a JEM2010 microscope operating at 200 kV. Prior to the TEM observation, small portions of the synthetic products were dispersed in ethanol and the suspension was deposited onto a holey carbon-coated copper grid.

[10] The low-field mass-specific magnetic susceptibility (χ) curve was measured using a Kappa bridge (KLY-3, sensitivity of 1×10^{-8} SI, AGICO Ltd., Brno, Czech Republic) at room temperature. Temperature dependence of magnetization (*J-T*) curve was measured in a steady field of 1 T from room temperature to 800°C, using a Magnetic Measurements Variable Field Translation Balance in air. The Curie temperature (T_c) was determined by the intersection of two tangent lines that bounded the T_c [*Moskowitz*, 1981].

[11] Hysteresis loops, were measured using a Quantum Design Magnetic Properties Measurement System (MPMS XL-5, with a sensitivity of 5.0×10^{-10} Am^2) at room temperature, with a maximum field of 5 T.

[12] First-order reversal curve (FORC) analyses were conducted using a Princeton Measurements Corporation vibrating sample magnetometer (Micromag VSM 3900) at room temperature. A total of 180 FORCs were measured with field up to 2.2 T for each sample, and then processed using software FORCinel version 1.17 [*Harrison and Feinberg*, 2008].

[13] Low-temperature properties of hematite were also measured using the MPMS XL-5 apparatus. First, saturated isothermal remanent magnetization (SIRM) was imparted with a 2.5 T field at room temperature ($SIRM_{300\ K}$). After the magnetic field was switched off, $SIRM_{300\ K}$ was cycled from 300 to 10 K and then from 10 to 300 K. In addition, the frequency dependence of magnetic susceptibility was also determined at 10 Hz from 300 to 10 K.

3. Results

3.1. Non-magnetic Analysis

[14] The Al content differed significantly for the two series of samples. For the HFh* samples, Al content ranged between 0 and 12.9 mol%, well below the upper limit of 15–16 mol% Al in synthetic Al-hematite formed from ferric solutions at low temperature [*Schwertmann et al.*, 1979; *Cornell and Schwertmann*, 2003]. In contrast, for the HGL* series samples, the Al content reached up to ~26.6 mol%, comparable to its precursor Al-goethite [*Cornell and Schwertmann*, 2003]. However, hematite obtained through heating Al-goethite at 800 °C can contain corundum (Al_2O_3) [*Wells*, 1989]; therefore, the level of Al substitution of HGL30 is likely to be overestimated. For HGH* series samples, the Al content was <6 mol% because aging of ferrihydrite in 5 M NaOH results in reduced incorporation of Al in goethite [*Lewis and Schwertmann*, 1979].

[15] The XRD patterns indicate that almost all samples were dominated by hematite, except for the sample HFh16, in which ferrihydrite was also present. This was due to the high concentration of Al in the initial system, which hindered the transformation of ferrihydrite into hematite [*Lewis and Schwertmann*, 1979]. Therefore, the sample HFh16 was not used for further analyses except for the unit-cell parameter determination.

[16] For each series samples, as Al substitution increased, the positions of the peaks in the XRD pattern shifted to higher angles and the peak intensities decreased (Figure 1). The unit cell edge length decreased linearly with increasing Al substitution (Table 2, Figures 3a and 3b), because Al^{3+} (0.53 Å) is smaller than Fe^{3+} (0.65 Å) [*Schulze*, 1984]. It should be highlighted that the unit cell parameters of HGL30 are similar to those of HGL20, which further confirms that HGL30 is the mixture of Al-hematite and corundum, so the data for this sample are not taken for the calculation of the regression line.

[17] The grain size distribution follows a slightly skewed normal distribution. For each sample, mean diameters and standard deviations were determined from at least 100 individual particles counted on the basis of TEM photos (Table 2). As anticipated, samples produced under different conditions possess diverse morphologies and mean particle sizes (Figures 2 and 3c). For instance, the crystal sizes of HFh* series samples are generally larger than those of HG* series. For the HFh* series, the particles are platy, their diameters increasing with increasing Al content. For the HGH* series, the particles are highly elongated as their morphologies are inherited from the precursor goethites even after 4 h of heating. In contrast, HGL* series are fine granular shaped as they were transformed from granular goethite. In addition, the length of major (or elongated) axis for HG* samples is smaller than the diameter of the HFh* samples.

3.2. Magnetic Analysis

[18] Raw hysteresis loops for representative samples are shown in Figure 4. If the loops are calibrated with the high slope estimated between 4 and 5 T, a decrease in magnetization between 1 and 2 T for HG* series samples except HGL0, HGL2, HGL4, HGH0, HGH4 is observed (see Figure S1 in the auxiliary material).[1] This behavior indicates that the hysteresis loops have been over-corrected because a high-coercivity component could co-exist. Then the loops of those samples were calibrated with the slope of 1–2 T, and two coercivity components were shown in loops as we expected (Figure 5). As Al content increases, the hysteresis loops convert from rectangles or box-shaped to wasp-waisted, and to ramp-shaped. Such conversion reflects changes in magnetic domain states from single-domain (SD) to mixtures of SD and superparamagnetic (SP), and then to entire SP grains [*Roberts et al.*, 1995; *Evans and Heller*, 2003; *Fabian*, 2003]. In addition, HG* series samples (except HGL0, HGL2, HGL4, HGH0, HGH4, HGH30) are not saturated even at 5 T. These loops indicate the existence of two distinctive coercivity components, one saturated around 1 T but the other far from saturation. The higher coercivity component is probably caused by the surface effect or the existence of exchange bias, which may be

[1] Auxiliary materials are available in the HTML. doi:10.1029/2011JB008605.

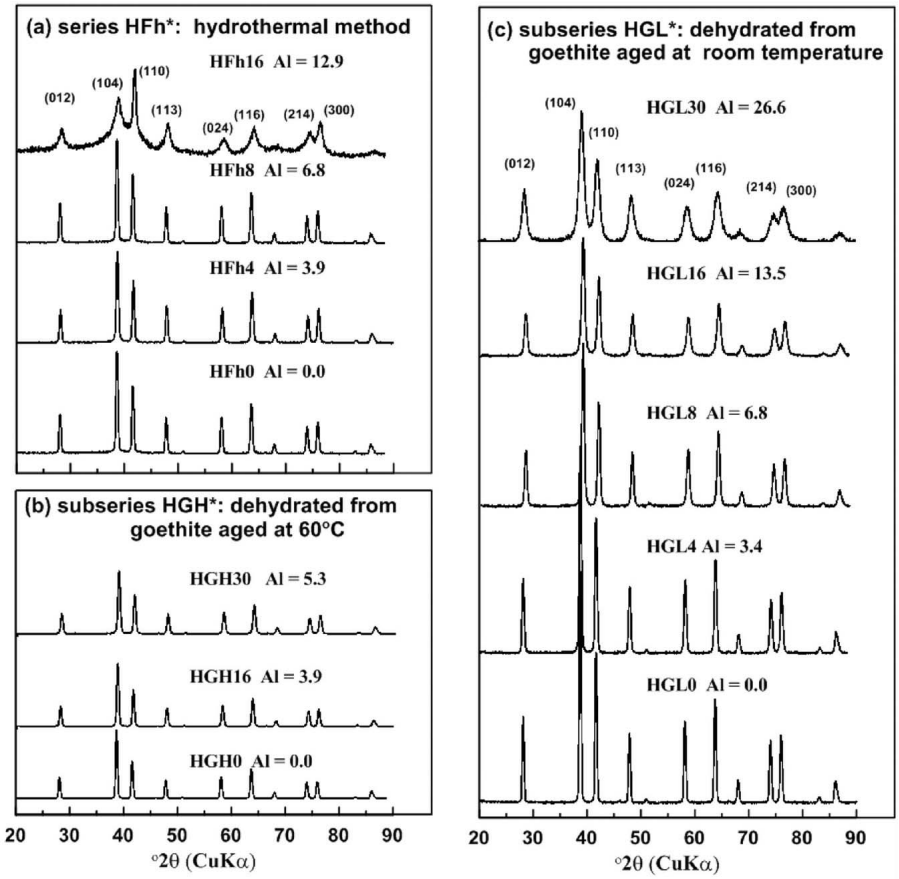

Figure 1. X-ray diffraction for two series of hematite samples. (a) Series HFh* samples were synthesized from ferrihydrite and the Al substitution for the four samples are 0, 3.9, 6.8 and 12.9 mol%, respectively. (b) Subseries HGH* samples were obtained by dehydroxylation of goethite synthesized from a Fe(III) salt aged at 60°C at high pH, and the Al substitution for the three samples is 0, 3.9 and 5.3 mol%, respectively. (c) Subseries HGL* samples were obtained by dehydroxylation of goethite prepared by precipitation and oxidation of a Fe (II) salt at room temperature. Five samples were chosen for the XRD measurements with putative Al substitution ranging from 0 to 26.6 mol%.

Table 2. Selected Properties of the Studied Hematite

Sample	Al (mol%)	*a* (nm)	*c* (nm)	Particle size (nm)	W(104)/W(110)	Room-T χ (10^{-8} kg^{-1} m^3)
HFh0	0.0	0.5037	1.3788	167.2 ± 50	1.01	410
HFh2	2.0	0.5034	1.3778		0.99	170
HFh4	3.9	0.5030	1.3811	219.8 ± 66.6	1.02	257
HFh8	6.8	0.5017	1.3675	358.1 ± 60.9	1.18	104
HFh16	13.0	0.5016	1.3706			210
HGH0	0.0	0.5020	1.3701	229.2 ± 77.1	0.99	52
HGH2	0.8	0.5014	1.3698		1.02	46
HGH4	1.5	0.5010	1.3688		1.01	32
HGH8	2.4	0.4996	1.3710		1.01	32
HGH16	3.9	0.5002	1.3699	122.6 ± 44.5	1.00	33
HGH20	4.9	0.5001	1.3682		1.04	29
HGH30	5.3	0.5003	1.3675	91.9 ± 31.2	1.04	26
HGL0	0.0	0.5014	1.3690	249.4 ± 81.2	1.02	40
HGL4	3.4	0.5009	1.3683		1.00	30
HGL8	6.8	0.4985	1.3700	66.3 ± 17.0	0.99	26
HGL16	13.5	0.4958	1.3718	42.1 ± 10.2	1.04	30
HGL20	15.8	0.4976	1.3696	32.2 ± 7.2	0.17	33
HGL30	26.6	0.4965	1.3675	20.8 ± 5.4	0.96	45

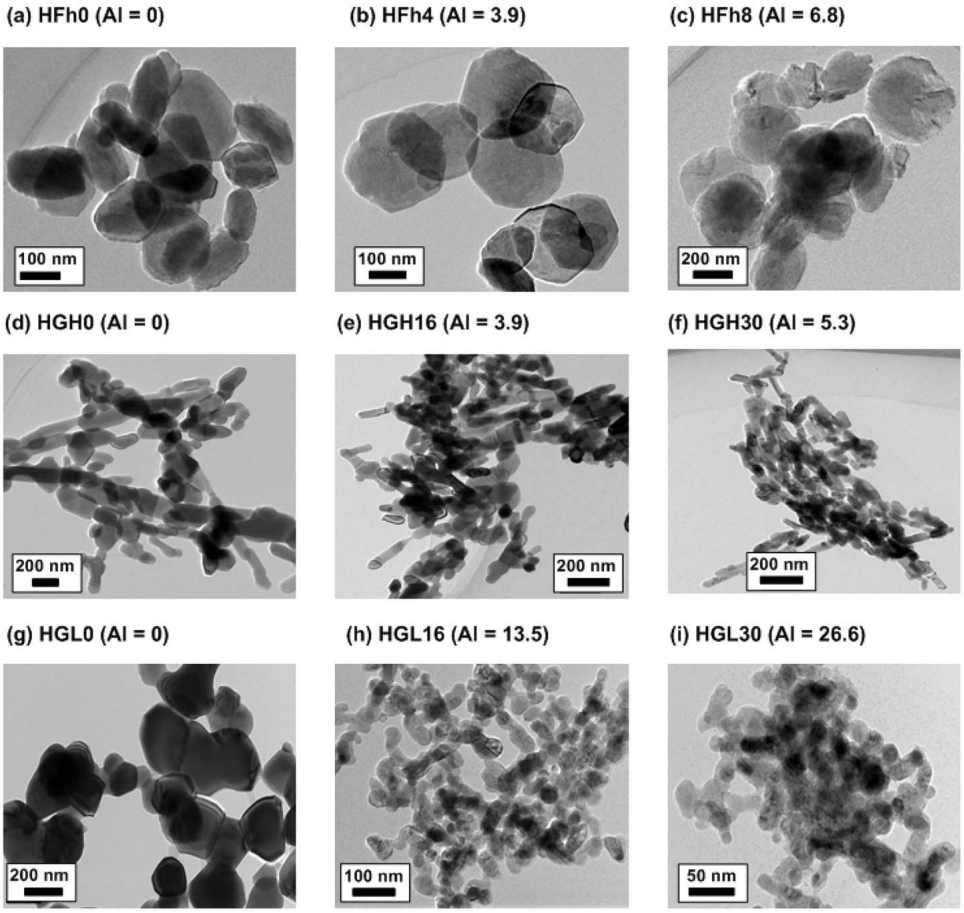

Figure 2. Transmission electron microscope observations for two series of hematite samples. The scale bar is 100 nm for (a) HFh0, (b) HFh4, (h) HGL16; 200 nm for (c) HFh8, (d) HGH0, (e) HGH16, (f) HGH30 and (g) HGL0; and 50 nm for (i) HGL30. The parentheses after sample names indicate the Al content in mol%.

attributed to a strong unidirectional anisotropy caused by the Al-ordering arrangement (Figure S2 in the auxiliary material) [*Fabian et al.*, 2008; *McEnroe et al.*, 2009]. Then, coercivity (B_c) and pseudo-saturated magnetization (PM_s, as it is not saturated absolutely) used in the following text are obtained from the first saturated component.

[19] For both HFh* and HGH* samples, B_c increases systematically with increasing Al content (Figures 5a–5f).

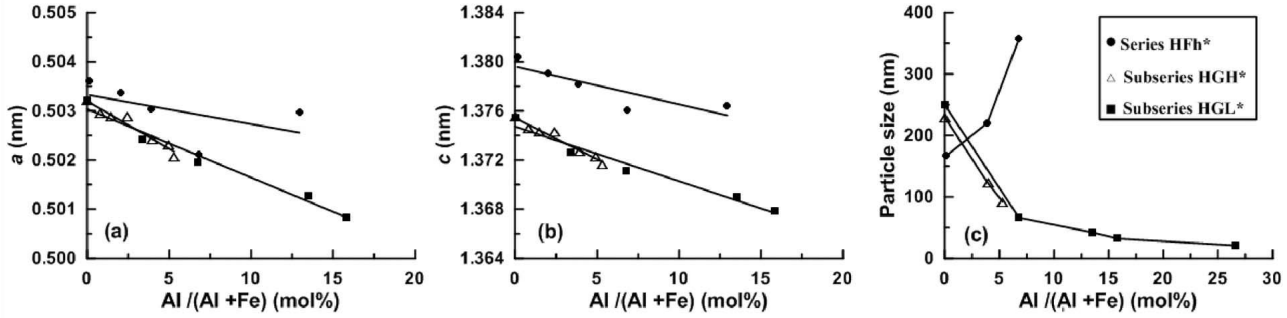

Figure 3. Aluminum (Al) substitution dependency of unit cell edge length (a, c) and particle size for synthetic hematite samples. (a) The unit cell edge length a versus Al substitution, where the solid lines represent the fitting curves for series HFh*, subseries HGH* and HGL*, and the R (relative coefficient) squares are 0.27, 0.63, 0.95. (b) The unit cell edge length c against Al content, the R squares for the solid fitting curves are 0.73, 0.96, 0.83. (c) Particle size versus Al substitution, where solid circle, empty triangle, and solid square represent series HFh*, subseries HGH* and HGL* samples, respectively. The data point for the sample with Al/(Fe + Al) = ~26 mol% was not taken for the calculation of the regression line (see text).

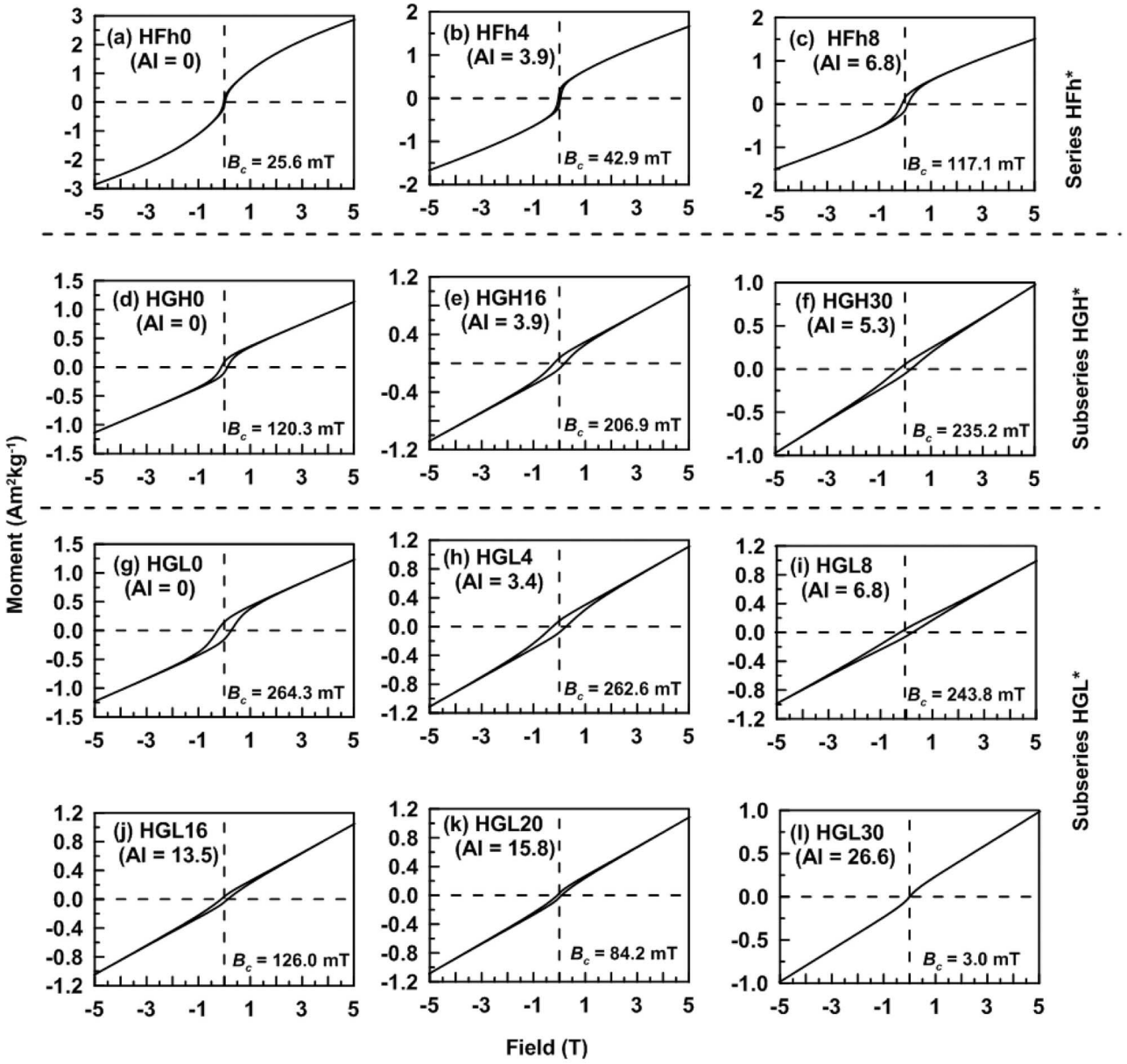

Figure 4. Raw hysteresis loops tested at room temperature for (a–c) series HFh* samples, (d–f) subseries HGH* samples, and (g–l) subseries HGL* samples. The parentheses after sample names indicate the Al content in mol%.

However, for the HGL* samples, B_c increases with Al substitution up to 6.8 mol%, and then decreases as Al concentration further increases (Figures 5g–5l). In general, HFh* samples exhibit lower coercivities than the HG* series samples. Sample HGL30 exhibits extremely apparent superparamagnetic (SP) behavior (Figure 5l).

[20] FORC diagrams for representative samples are shown in Figure 6. For the HFh* samples, little vertical spread of the contours was observed in the FORC diagrams, indicating that magnetostatic interactions are negligible. In contrast, the vertical spreads of the contours for samples HGH0, HGL0 and HGH16, HGH30 are ~200 mT. The seemingly larger magnetic interaction field is caused by the smoothing factor (SF > 9). Another notable feature of these FORC diagrams is a systematically higher mean coercivity peak and wider coercivity distribution with increasing Al content, except for samples with Al concentration > 13.5 mol% (Figure 6).

[21] *J-T* curves are shown in Figure 7. For series HFh* samples (Figures 7a–7c), an overall decrease in magnetization is observed, and the heating and cooling curves are irreversible below 400°C. While for series HG* samples, the heating curves (Figures 7d–7g), except for HGL30, show initially a gradual increase of magnetization with temperature, and then decrease in magnetization up to T_c. For sample HGL30 (Figure 7h), the heating curve decreases linearly with temperature below T_c. These complicated features indicate that some mineral transformation could have

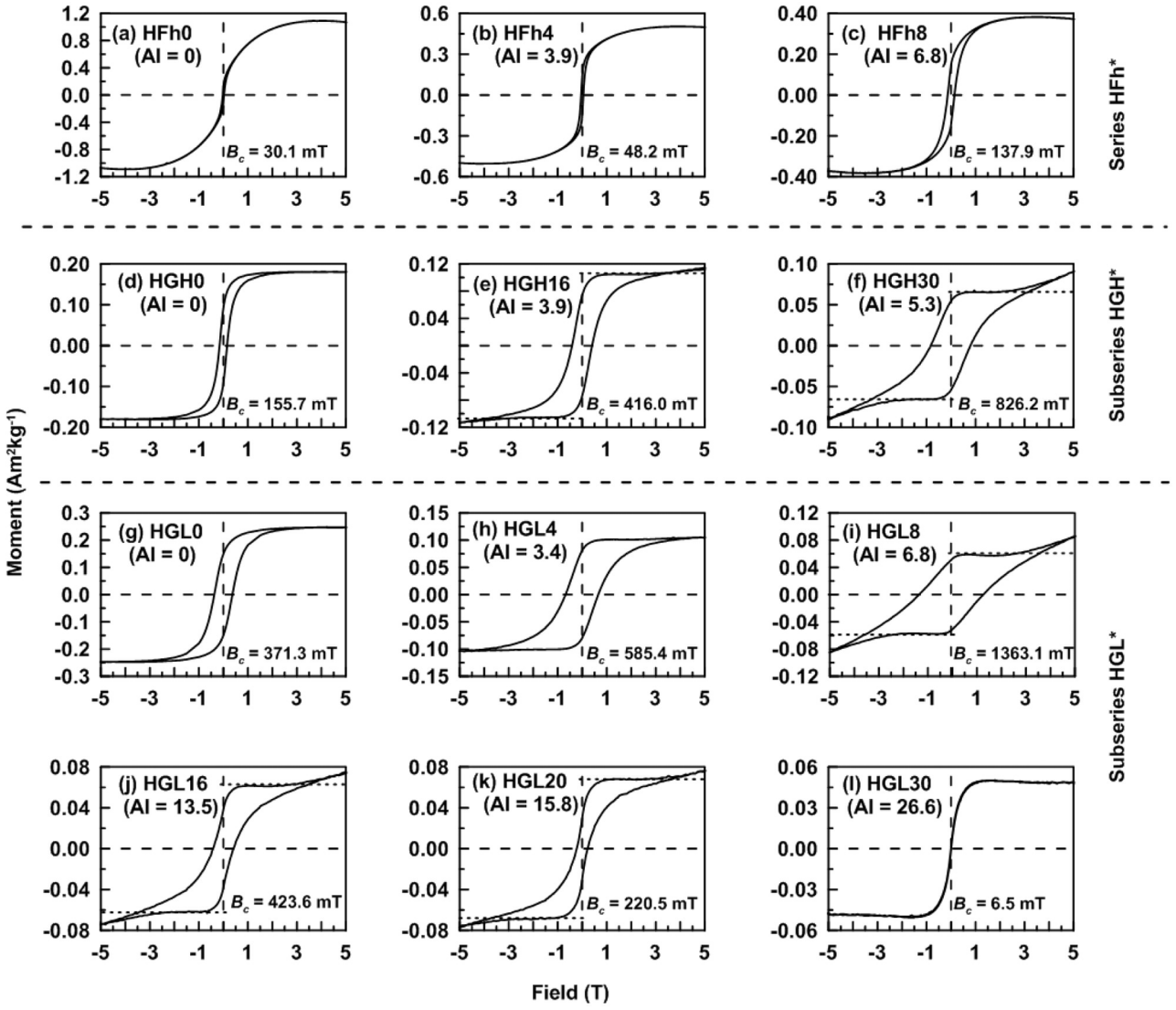

Figure 5. Room temperature hysteresis loops after removal of the high-field component (see text for details) for (a–c) series HFh* samples, (d–f) subseries HGH* samples, and (g–l) subseries HGL* samples. The parentheses after sample names indicate the Al content in mol%.

occurred upon heating, but this does not affect the determination of T_c.

[22] No apparent Morin transitions were observed in the low temperature SIRM cycles for series HFh* samples (Figures 8a–8c), which was rather related to the incorporated water and OH groups [*Dang et al.*, 1998; *Vandenberghe et al.*, 2000]. On the other hand, for series HG* samples, Morin transitions are well defined in SIRM cycle curves for samples with lower degree of Al substitution. In addition, the Morin transition temperature shifts to lower temperatures as the Al content increases, and the Morin transition disappears as Al content exceeds 13.5 mol%, which is consistent with the Mössbauer result of *de Grave et al.* [2002]. Although the influence from grain size, morphology and the presence of defects cannot be ignored, Al-for-Fe substitution is the most important parameter in determining the Morin transition temperature [*de Grave et al.*, 2002].

[23] The low temperature dependence of in-phase susceptibility is showed in Figure 9. Morin transitions are absent for series HFh* samples, but some peaks at 20–30 K have been detected which may be the blocking temperature for finer ferrihydrite hidden in hematite. For series HG* samples, clear Morin transitions are observed. Meanwhile, Morin transition disappears while Al concentration reaches 13.5 mol%. In addition, the susceptibility curve for HGL30 exhibits a peak around 120 K, which is likely related to the unblocking process.

[24] The χ values at room temperature are Al-dependent for the two series samples (Figure 10a). When Al content is $<\sim$7 mol%, χ is negatively correlated with the Al content, and then χ increases with further increasing the Al content. The B_c curves exhibits a mirror relationship with respect to the Al content compared to χ. In addition, the susceptibility for series HFh* samples is at least eight times larger than that of series HG* samples, suggesting that the

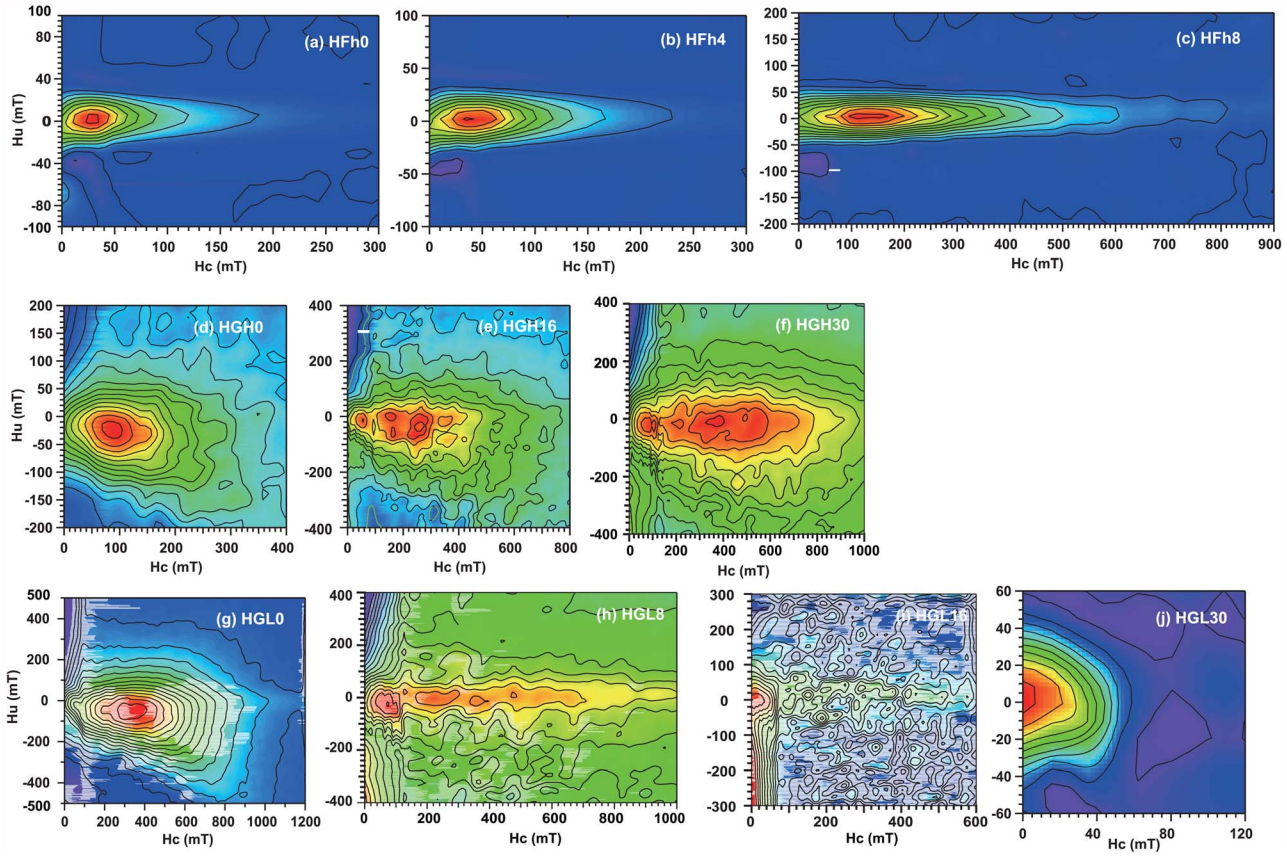

Figure 6. FORC diagrams for synthetic aluminous hematite samples, where each horizontal row of diagrams represents the same series samples. The parentheses after sample names indicate the Al content in mol%.

magnetization of series HFh* samples is stronger than that of the series HG* samples.

4. Discussion

4.1. Effects of the Al Substitution on the Properties of Hematite

[25] Magnetic properties of hematite depend on the crystallinity, average particle size and morphology of hematite crystals [*Dunlop*, 1971; *Cornell and Schwertmann*, 2003]. Moreover, these properties are further controlled by the degree of Al substitution. Therefore, magnetic properties of hematite show systematic variations with Al content.

[26] First of all, consistent with previous studies [*Schwertmann et al.*, 1979; *Taylor and Schwertmann*, 1980; *Barrón et al.*, 1984; *Schulze*, 1984; *Stanjek and Schwertmann*, 1992], the cell edge lengths a and c decrease with increasing Al substitution (Figures 3a and 3b). The grain size of the Al-hematite also gradually decreases with increasing Al substitution. For pure hematite without cation substitution, the SP/SD threshold is 20–30 nm, while the upper SD limit is $\sim$15 μm [*Dunlop and Özdemir*, 1997; *Kletetschka and Wasilewski*, 2002]. At the SP/SD threshold, the grain size-dependent properties (e.g., χ and B_c) change dramatically. Therefore, it is practical to estimate the SP/SD threshold using the grain size-dependence of χ and B_c [*Maher*, 1988; *Liu et al.*, 2005]. Figure 3c reveals that the grain size for the HGL* samples sharply decreases from several hundreds of nanometers down to several tens of nanometers when the Al content is $>\sim$5 mol%. The hysteresis loops change suddenly from typical SD behavior for HGL20 (B_c = 220.5 mT) to more SP-like (B_c = 6.5 mT) for HGL30 (Figure 5), the corresponding particle size decreasing from 32.2 to 20.8 nm. Therefore, the SP/SD threshold for Al-hematite falls between HGL20 (32.2 nm) and HGL30 (20.8 nm), and is comparable with that of hematite without cation-substitution (20–30 nm), but the precise SP/SD threshold for Al-hematite is beyond the scope of the present study.

[27] Above the SP/SD threshold, when Al content is $<\sim$7$-$8 mol%, hematite is situated well in SD grain size region. Then we observe a positive correlation between B_c and the Al content (Figure 10c). This is mainly attributed to the development of lattice defects arising from the incorporation of Al [*Wells et al.*, 1999] or internal stress [*Stanjek and Schwertmann*, 1992; *Hansen et al.*, 2000; *Liu et al.*, 2008]. The development of the defect caused by incorporation of Al inhibits magnetic domain rotation or flipping, resulting in an increase in magnetic hardness (i.e., magnetic coercivity), and lowering the magnetic susceptibility (Figures 10a and 10c).

[28] Unlike χ and B_c, the magnetization displays different variation pattern (Figure 10b). Hematite has a rhombohedral crystal structure isomorphous with corundum [*Morrish*, 1994; *Hansen et al.*, 2000; *Cornell and Schwertmann*, 2003]. Below

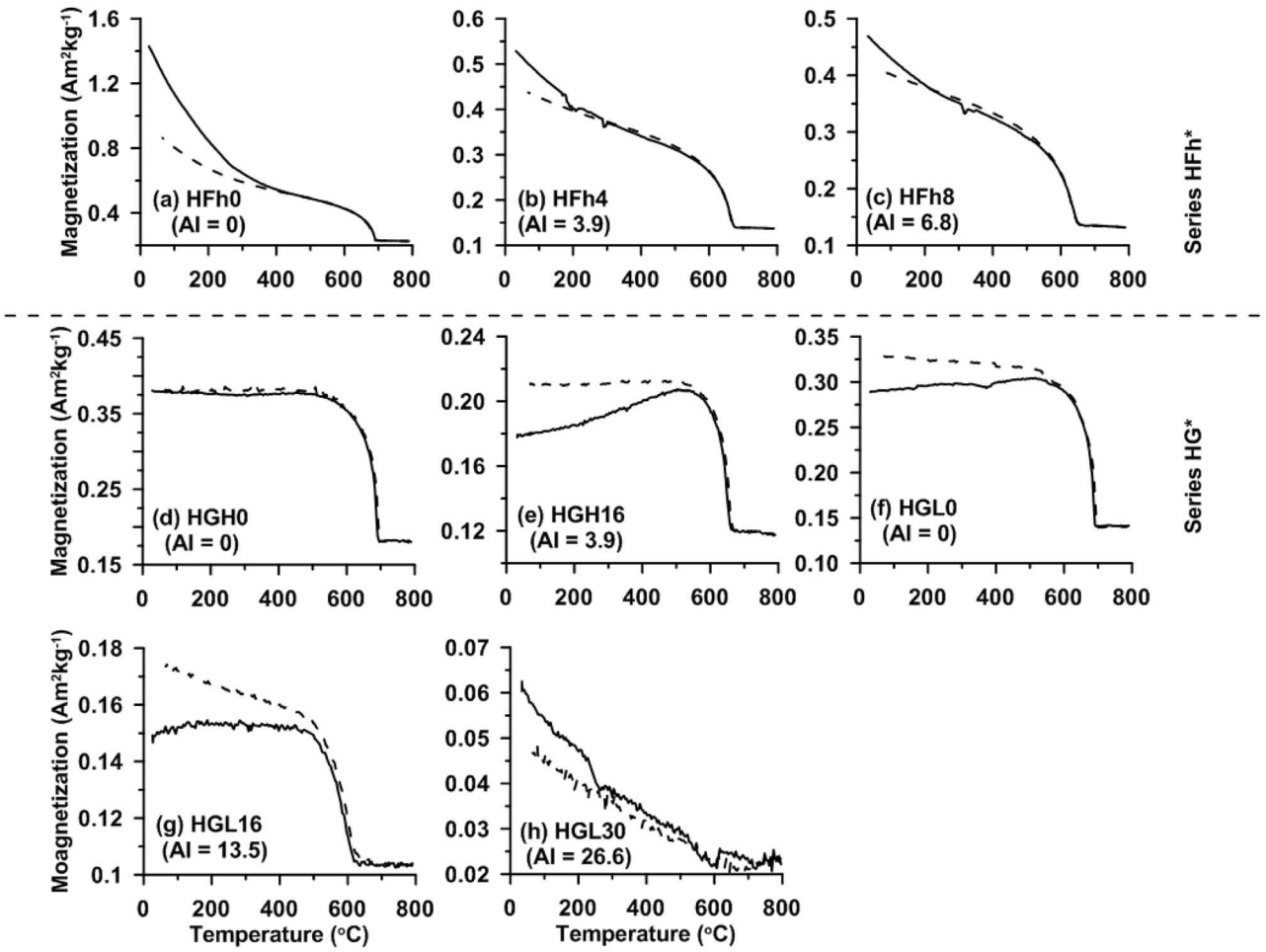

Figure 7. Temperature dependence of magnetization (*J–T*) for some representative samples, which were measured in a steady field of 1 T from room temperature to 800°C in air. The solid and dashed lines indicate the heating and cooling curves, respectively. The parentheses after sample names indicate the Al content in mol%.

the Morin transition, the spins on the two adjacent Fe layers (A and B layers) are arranged oppositely along the c-axis with equal probabilities, completing the antiferromagnetism of hematite. However, once the temperature exceeds the Morin temperature, an antiferromagnetic spin flop occurs. The spins of two adjacent layers are pinned in the rhombohedral c-plane, within which they are canted out of exact antiparallelism by a small angle, and then results in a net canted antiferromagnetism [*Dzyaloshinsky*, 1958; *Moriya*, 1960; *Özdemir and Dunlop*, 2002, 2005, 2006; *Liu et al.*, 2007; *Özdemir et al.*, 2008]. In addition, although the spin-canted ferromagnetism vanishes below Morin temperature, an isotropic ferromagnetism, defect moment still exists, which originates from chemical or lattice defects [*Smith and Fuller*, 1967; *Dunlop*, 1971; *Bucur*, 1978; *Özdemir and Dunlop*, 2006]. As a result, the total magnetization for hematite is the combination of spin-canted moment and defect moment. As defined by *Özdemir and Dunlop* [2006], the defect moment was designated as the remanent magnetization below Morin transition. For HGL30 that does not show any sign of the Morin transition, the remanent magnetization at 10 K was used. Practically, such approximation does not influence the overall trend of defect moment to Al content.

[29] Figure 10e shows the relationship between the defect moment and the Al concentration for HG* series samples. The result displays that the defect moment increases as the Al concentration increases to 13.5 mol%. This behavior demonstrates that Al is preferentially incorporated into the two sub-lattice layers. However, once the Al concentration exceeds 13.5 mol%, the defect moment decreases, which can be reasonably interpreted by the dilution effects of Al.

[30] Unlike the defect moment, the room temperature (RT) PM_s, decreases systematically with increasing Al substitution in the two series (Figure 10b). On the contrary, an opposite trend was observed for the defect moment. Although PM_s is dependent both on the defect moment and spin-canted moment, it is likely that the RT PM_s are mostly governed by the spin-canted moment. After all, the spin-canted moment has been diluted by Al as the Al content increases.

[31] Two-tangent method has been used to determine the Curie temperature of these samples [*Moskowitz*, 1981]. The T_c against Al concentration diagrams (Figure 10d) show that

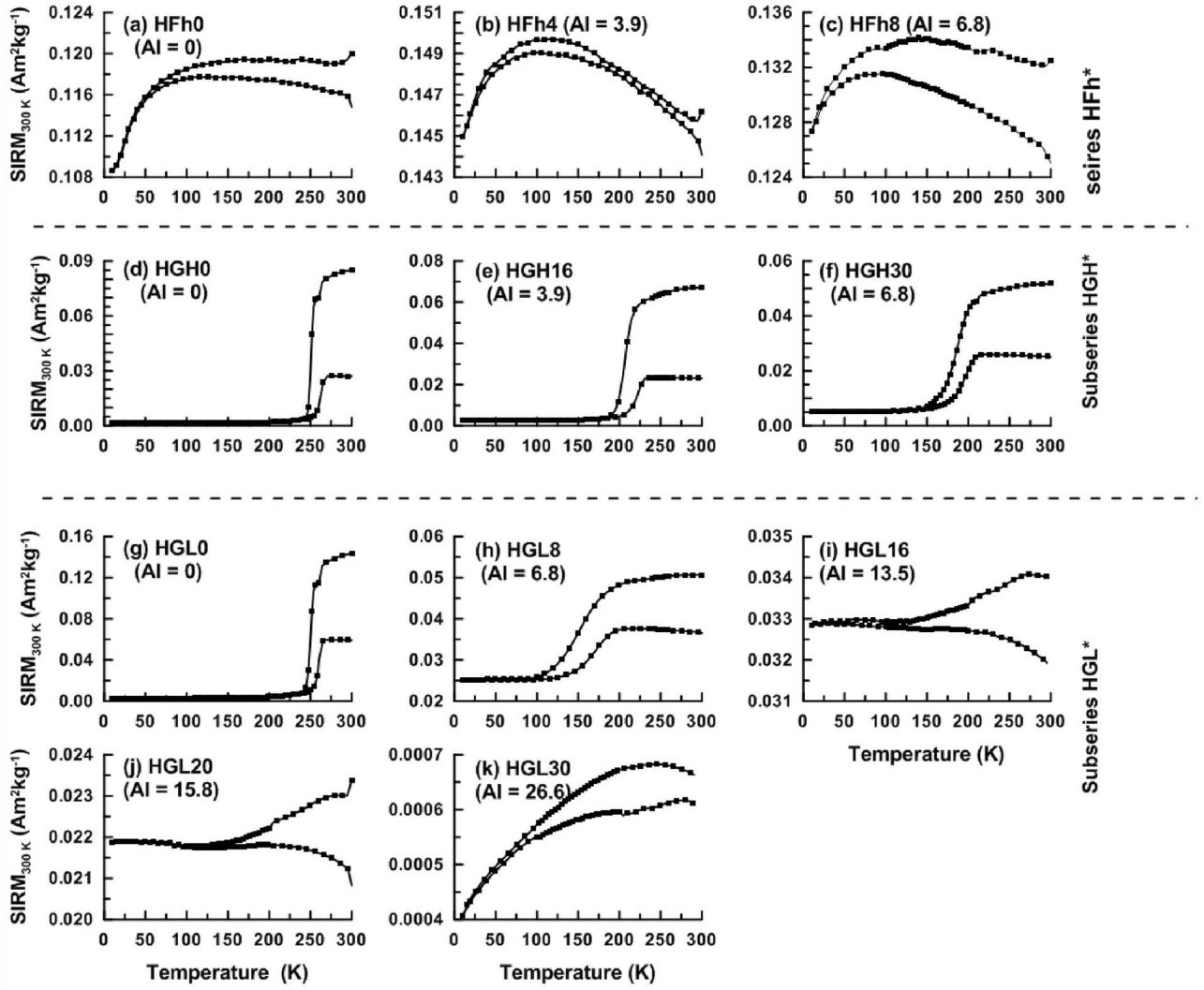

Figure 8. Temperature dependence of SIRM produced by a 2.5 T field applied at 300 K, during zero-field cooling from 300 to 10 K and warming back to 300 K. (a–c) For samples from series HFh*, Morin transition is undetectable; while (d–k) for samples from series HG*, clear Morin transition is observed. The parentheses after sample names indicate the Al content in mol%.

the Curie temperature steadily decreases as Al substitution increases, which may be due to the newly formed lattice defects caused by Al substitution. In addition, based on the diagram between T_c and Al content, HGL30, a mixture of Al-hematite and Al_2O_3, should possess higher Al concentration than HGL20, as T_c of HGL30 is lower than that of HGL20. Therefore, it seems that T_c is more sensitive to the Al content than the unit cell parameters when the Al content is $>\sim$16 mol%.

4.2. Discrimination of Hematites Synthesized by Hydrothermal and Dehydroxylation Methods

[32] The properties of these two series of hematite differ significantly. First, the grain morphologies are completely diverse. For series HFh* samples, particles are definitely oblate in shape. In addition, the particle size increases with increasing Al substitution. The WHH(104)/WHH (110) data show that the series HFh* particles tend to be relatively thinner and larger as Al content increases, consistent with the TEM observations (Figure 2). In other words, Al substitution inhibits the growth in the crystallographic z-direction for series HFh* samples. For series HG* samples, the particles are elongated, slender and, moreover, particle size decreases with increasing of Al content, which is attributed to its precursor goethite, whose growth is hindered by Al incorporation [*Schulze*, 1984; *Cornell and Schwertmann*, 2003]. Indeed, the ratios of widths to height are close to 1 except for HGL20, indicating a lack of significant anisotropic growth.

[33] Second, the HFh* series hematite are magnetically stronger (i.e., higher magnetization) but softer (i.e., lower magnetic coercivity) than the HG* series samples (Figures 10a and 10c). For instance, nearly three to fourfold intense PM_s were observed for HFh* than the HG* series for the similar Al content. Such a large discrepancy in magnetic capacity possibly originates from the degree of unbalance of Al atoms in the A and B layers. It is likely that dehydration of goethite allows more ordered distribution of Al atoms in

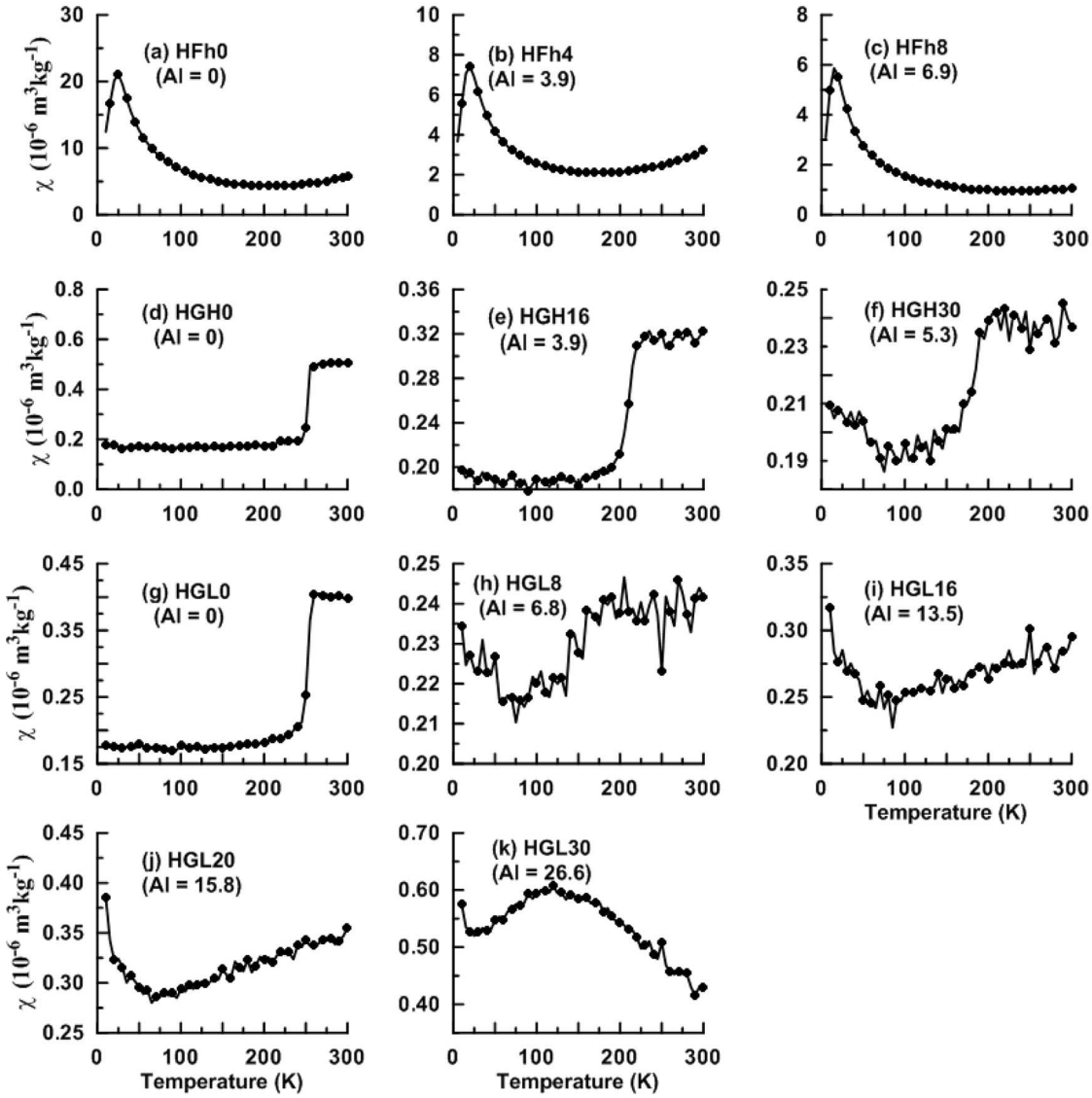

Figure 9. Temperature dependence of in-phase magnetic susceptibility for different series samples determined at 10 Hz from 300 to 10 K. The parentheses after sample names indicate the Al content in mol%.

alternating crystal lattice rather than the hydrothermal transformation of ferridydrite. If so, higher unbalance of Al atoms in HFh* series samples results in a larger net magnetization than HG* series samples. In addition, the higher temperature during crystal formation probably induced some degree of recrystallization of the HG* series samples and annealed the defects out of the structure, diminishing the contribution of the defect moment to the magnetization [*Dunlop*, 1971; *de Boer and Dekkers*, 1998, 2001].

[34] *Michel et al.* [2010] and *Cabello et al.* [2009] demonstrated that an intermediate ordered ferromagnetic ferrihydrite occurs through the hydrothermal transformation from 2-line ferrihydrite to hematite. Then a minimum residue of this ferromagnetic intermediate phase could partly contribute to the room-T magnetization for the hydrothermal hematite as evident by the irreversible *J-T* behavior below 400°C because such a phase is thermally unstable [*Liu et al.*, 2008]. By comparing the warming and cooling *J-T* curves (Figure 7), this phase contributes less than 20% of the room-T magnetization. Therefore, the stronger magnetization for HFh* series hematite is still attributed to the effects of Al-substitution.

[35] Contrary to magnetization, magnetic coercivity was lower for series HFh* samples than for HG* samples (Figures 10b and 10c), because the magnetic coercivity in hematite mostly originates from the induced magnetic anisotropy which is inversely proportional to the saturated magnetization [*Porath*, 1968]. In addition, morphologic contribution from the elongated shape anisotropy also favors higher magnetic coercivity for HG* series samples.

[36] Finally, the two series are clearly distinctive in a correlation diagram between T_c and unit cell edge length c (Figure 11a). The diagram has been divided into four quadrants with vertical (c = 1.376 nm) and horizontal (T_c = 640°C) lines. Series HFh* data points are mainly located in the upper right quadrant, while series HG* data points are located in the two left quadrants. This suggests that the Curie

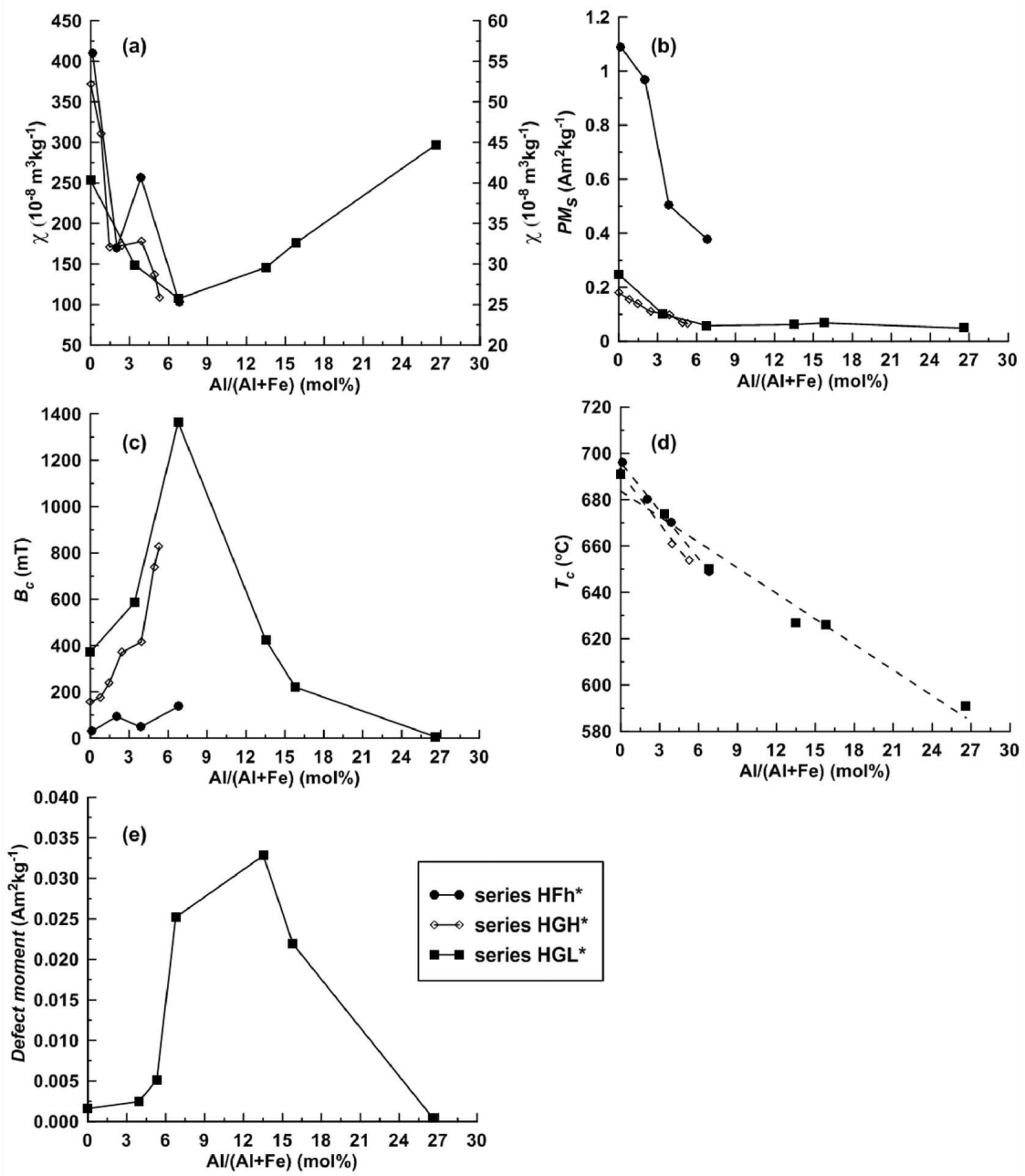

Figure 10. Correlation diagrams for magnetic parameters versus Al concentration, where solid circle, empty diamond, and solid square represent series HFh*, subseries HGH* and HGL* samples. (a) χ versus Al/(Al + Fe), where the left axis represents the data for series HFh*, while the right axis is for series HG*; (b) PM_s to Al/(Al + Fe); (c) B_c to Al/(Al + Fe); (d) T_c to Al/(Al + Fe), and the dash lines stand for the fitting curves for T_c to Al concentration; (e) Defect moment to Al/(Al + Fe) for series HG* samples.

point versus edge parameter (c) can help diagnose the origin of hematite.

4.3. Geological Significance

[37] Hematite, which is the second most common Fe oxide in terrestrial soils, can be formed by a variety of geologic routes [*Schwertmann and Cornell*, 2000]. In this study, however, we focused on hematite formed by hydrothermal transformation of ferrihydrite and thermal dehydroxylation of goethite. The discrimination of these two kinds of hematite is useful to deduce their generation environments. The detection of goethite-transformed hematite can be used as an indicator for the occurrence of fire, especially forest fire, or the combustion of coal seams because goethite transforms into hematite under heating [*de Boer et al.*, 2001; *Nørnberg et al.*, 2004, 2009]. On the other hand, hematites produced from hydrothermal transformation of ferrihydrite are similar to those typically formed in soils of temperate and warm regions subjected to wet-dry cycles. *Liu et al.* [2010] investigated three red soil sections in South China, and found hematite to be the dominant magnetic carrier.

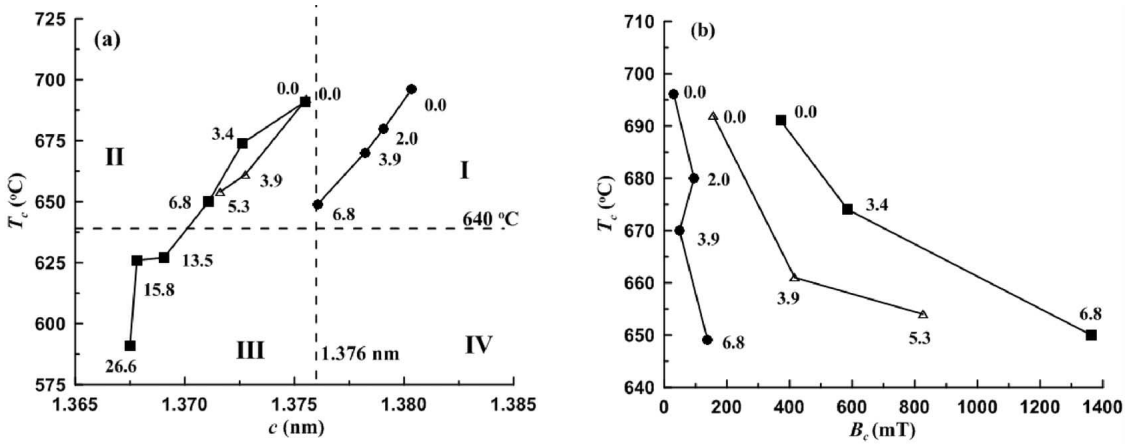

Figure 11. The correlation diagrams for T_c versus (a) c and (b) B_c. The numeral values in diagrams stand for the Al concentration of samples, with mol% as unit. In addition, I, II, III and IV indicate the four areas, divided by horizontal line (T_c = 640°C) and vertical line (c = 1.376 nm). Further, the solid circle, empty triangle, and solid square indicate series HFh*, subseries HGH* and HGL* samples, respectively.

Based on the magnetic properties of samples (T_c at 630–640°C and low B_c (<50 mT)), *Liu et al.* [2010] interpreted hematite in these sections to be mainly originated from ferrihydrite, which is in agreement with the local climate (seasonal dry-wet alternation coupled with high mean annual temperature and low mean annual precipitation).

[38] The estimated Curie point of hematite is notoriously diverse, being sometimes confused with that for maghemite or even magnetite [*Butler*, 1992; *Tauxe*, 2010]. In the present study, the T_c values are dependent on the amount of Al substitution. For instance, the correlation diagram between T_c and Al concentration (Figure 10d) reveals that the observed T_c values for Al substitution <16 mol% are all >610°C, well above the Curie point of magnetite. For hematite produced from ferrihydrite crystallization, Al content is usually <16 mol %, and the corresponding T_c is > ~620°C, again well above the Curie point of magnetite. The only worry is a goethite with >26.6 mol% Al, whose Curie point is similar to that for magnetite. However, nominal heat treatment during thermal demagnetization will transform it into high-Al hematite with proximal grain size of SP/SD threshold, thus will not contribute to the paleomagnetic signal.

[39] The T_c-B_c diagram (Figure 11b) shows that T_c is negatively related with B_c for different series of samples. It is well defined that the unblocking temperature T_b is always less than the Curie temperature T_c. In addition, with increasing the Al-content, the grain size (volume, which is usually positively correlated to T_b) of Al-hematite also decreases. By integrating these two factors, T_b of Al-hematite should be also negatively related with B_c. In contrast, for pure (Al-free) hematite, the unblocking temperature, T_b, increases with grain size (volume) [*Mørup et al.*, 2007; *Bedanta and Kleemann*, 2009]. Meanwhile, between the SP/SD threshold (~20–30 nm) and the SD/PSD threshold (about several tens of μm), B_c of hematite is also positively correlated to its grain size (see Figure S3 in the auxiliary material) [*Chevallier and Mathieu*, 1943; *Banerjee*, 1971; *Kletetschka and Wasilewski*, 2002]. Therefore, T_b and B_c are in a positive correlation for pure SD hematite. Similarly, it can be proposed that a correlation of T_b and B_c can diagnose the origin of SD hematite in nature. In summary, a positive link between T_b and B_c suggests the presence of pure SD hematite without cation substitution, while a negative trend indicates an Al-substituted SD hematite of chemical origin.

5. Conclusions

[40] Mineralogic and magnetic investigations were carried out on hematites produced from two different methods. The HFh* series hematite was produced by hydrothermal transformation from ferrihydrite while the HG* series samples by dehydration from goethite.

1. The HFh* series samples display plate-like morphologies, but the HG* series samples exhibit elongated morphologies with smaller average particle size.

2. The HFh* series samples display higher saturation magnetization but lower magnetic coercivity than that of HG* series samples. Lattice unbalance of Al substitution during transformation from ferrihydrite induces stronger magnetization for HFh* series samples. Lower magnetic coercivities for HFh* series samples are also natural since magnetic coercivity inversely correlates with the saturation magnetization.

3. Linkage between T_b and B_c can diagnose the origin of SD hematite in nature. While a negative correlation is indicative of SD Al-substituted hematite of chemical origin, a positive link is a hallmark for the presence of pure (Al-free) SD hematite without ion substitution.

[41] **Acknowledgments.** This study was supported by the National Natural Science Foundation of China (grants 41025013, 40974036 and 40821091). Q. S. Liu acknowledges further support from the 100-talent Program of the Chinese Academy of Sciences. J. Torrent and V. Barrón were partly supported by Spain's Ministerio de Educación y Ciencia, Project CGL2010–15067, and the European Regional Development Fund. We thank useful discussions with Mark Dekkers on the high-field removal of hysteresis loops. Comments from two anonymous referees, Erwin Appel (Associate Editor), and André Revil (Editor) greatly improved the manuscript.

References

Banerjee, S. K. (1971), New grain size limits for palaeomagnetic stability in haematite, *Nature*, *232*, 15–16.

Barrón, V., J. Rendón, J. Torrent, and C. Serna (1984), Relation of infrared, crystallochemical, and morphological properties of Al-substituted hematites, *Clays Clay Miner.*, *32*(6), 475–479, doi:10.1346/CCMN.1984.0320605.

Bedanta, S., and W. Kleemann (2009), Topical review: Supermagnetism, *J. Phys. D Appl. Phys.*, *42*, 013001, doi:10.1088/0022-3727/42/1/013001.

Bucur, I. (1978), Experimental study of the origin and properties of the defect moment in single domain haematite, *Geophys. J. R. Astron. Soc.*, *55*(3), 589–604.

Butler, R. F. (1992), *Paleomagnetism: Magnetic Domains to Geologic Terranes*, Blackwell Sci., Oxford, U. K.

Cabello, E., M. P. Morales, C. J. Serna, V. Barrón, and J. Torrent (2009), Magnetic enhancement during the crystallization of ferrihydrite at 25 and 50°C, *Clays Clay Miner.*, *57*, 46–53, doi:10.1346/CCMN.2009.0570105.

Chevallier, R., and S. Mathieu (1943), Proprietes magnetiques des poudres d'hematite-influence des dimensions des grains, *Ann. Phys.*, *18*, 258–288.

Christensen, P. R., et al. (2000), Detection of crystalline hematite mineralization on Mars by the Thermal Emission Spectrometer: Evidence for near-surface water, *J. Geophys. Res.*, *105*(E4), 9623–9642, doi:10.1029/1999JE001093.

Christensen, P. R., R. V. Morris, M. D. Lane, J. L. Bandfield, and M. C. Malin (2001), Global mapping of Martian hematite mineral deposits: Remnants of water-driven processes on early Mars, *J. Geophys. Res.*, *106*(E10), 23,873–23,885, doi:10.1029/2000JE001415.

Cornell, R. M., and U. Schwertmann (1979), Influence of organic anions on the crystallization of ferrihydrite, *Clays Clay Miner.*, *27*, 402–410, doi:10.1346/CCMN.1979.0270602.

Cornell, R. M., and U. Schwertmann (2003), *The Iron Oxides Structure, Properties, Reactions, Occurrence and Uses*, VCH Weinheim, New York.

Dang, M. Z., D. G. Rancourt, J. E. Dutrizac, G. Lamarche, and R. Provencher (1998), Interplay of surface conditions, particle size, stoichiometry, cell parameters, and magnetism in synthetic hematite-like materials, *Hyperfine Interact.*, *117*, 271–319, doi:10.1023/A:1012655729417.

de Boer, C. B., and M. J. Dekkers (1998), Thermomagnetic behaviour of haematite and goethite as a function of grain size in various non-saturating magnetic fields, *Geophys. J. Int.*, *133*, 541–552, doi:10.1046/j.1365-246X.1998.00522.x.

de Boer, C. B., and M. J. Dekkers (2001), Unusual thermomagnetic behaviour of haematites: Neoformation of a highly magnetic spinel phase on heating in air, *Geophys. J. Int.*, *144*, 481–494, doi:10.1046/j.0956-540X.2000.01333.x.

de Boer, C. B., M. J. Dekkers, and T. A. M. van Hoof (2001), Rock-magnetic properties of TRM carrying baked and molten rocks straddling burnt coal seams, *Phys. Earth Planet. Inter.*, *126*(1–2), 93–108, doi:10.1016/S0031-9201(01)00246-1.

de Grave, E., C. A. Barrero, G. M. da Costa, R. E. Vandenberghe, and E. van San (2002), Mössbauer spectra of α- and γ-polymorphs of FeOOH and Fe_2O_3: Effects of poor crystallinity and of Al-for-Fe substitution, *Clay Miner.*, *37*(4), 591–606, doi:10.1180/0009855023740062.

Diakonov, I., I. Khodakovsky, J. Schott, and E. Sergeeva (1994), Thermodynamic properties of iron oxides and hydroxides. I. Surface and bulk thermodynamic properties of goethite (alpha-FeOOH) up to 500 K, *Eur. J. Mineral.*, *6*(6), 967–983.

Drodt, M., A. X. Trautwein, I. König, E. Suess, and C. B. Koch (1997), Mössbauer spectroscopic studies on the iron forms of deep-sea sediments, *Phys. Chem. Miner.*, *24*(4), 281–293, doi:10.1007/s002690050040.

Dunlop, D. J. (1971), Magnetic properties of fine-particle hematite, *Ann. Geophys.*, *27*(3), 269–293.

Dunlop, D. J., and Ö. Özdemir (1997), *Rock Magnetism: Fundamentals and Frontiers*, Cambridge Univ. Press, New York, doi:10.1017/CBO9780511612794.

Dzyaloshinsky, I. (1958), A thermodynamic theory of "weak" ferromagnetism of antiferromagnetics, *J. Phys. Chem. Solids*, *4*(4), 241–255, doi:10.1016/0022-3697(58)90076-3.

Eren, M., and S. Kadir (1999), Colour origin of upper cretaceous pelagic red sediments within the Eastern Pontides, northeast Turkey, *Int. J. Earth Sci.*, *88*(3), 593–595, doi:10.1007/s005310050287.

Evans, M. E., and F. Heller (2003), *Environmental Magnetism: Principles and Applications of Enviromagnetics*, Academic, Amsterdam.

Fabian, K. (2003), Some additional parameters to estimate domain state from isothermal magnetization measurements, *Earth Planet. Sci. Lett.*, *213*(3–4), 337–345, doi:10.1016/S0012-821X(03)00329-7.

Fabian, K., S. A. McEnroe, P. Robinson, and V. P. Shcherbakov (2008), Exchange bias identifies lamellar magnetism as the origin of the natural remanent magnetization in titanohematite with ilmenite exsolution from Modum, Norway, *Earth Planet. Sci. Lett.*, *268*, 339–353, doi:10.1016/j.epsl.2008.01.034.

Hansen, M. F., C. Bender Koch, and S. Morup (2000), Magnetic dynamics of weakly and strongly interacting hematite nanoparticles, *Phys. Rev. B Condens. Matter.*, *62*(2), 1124–1135, doi:10.1103/PhysRevB.62.1124.

Harrison, R., and J. Feinberg (2008), FORCinel: An improved algorithm for calculating first-order reversal curve distributions using locally weighted regression smoothing, *Geochem. Geophys. Geosyst.*, *9*, Q05016, doi:10.1029/2008GC001987.

Iglesias, T., V. Cala, and J. Gonzalez (1997), Mineralogical and chemical modifications in soils affected by a forest fire in the Mediterranean area, *Sci. Total Environ.*, *204*(1), 89–96, doi:10.1016/S0048-9697(97)00173-3.

Ketterings, Q. M., J. M. Bigham, and V. Laperche (2000), Changes in soil mineralogy and texture caused by slash-and-burn fires in Sumatra, Indonesia, *Soil Sci. Soc. Am. J.*, *64*(3), 1108–1117, doi:10.2136/sssaj2000.6431108x.

Kletetschka, G., and P. J. Wasilewski (2002), Grain size limit for SD hematite, *Phys. Earth Planet. Inter.*, *129*(1–2), 173–179, doi:10.1016/S0031-9201(01)00271-0.

Lewis, D., and U. Schwertmann (1979), The influence of aluminum on the formation of iron oxides. IV. The influence of [A1], [OH], and temperature, *Clays Clay Miner.*, *27*, 195–200, doi:10.1346/CCMN.1979.0270304.

Liu, C., C. Deng, Q. S. Liu, L. Zheng, W. Wang, X. Xu, S. Huang, and B. Yuan (2010), Mineral magnetism to probe into the nature of palaeomagnetic signals of subtropical red soil sequences in southern China, *Geophys. J. Int.*, *181*(3), 1395–1410.

Liu, Q. S., J. Torrent, B. A. Maher, Y. Yu, C. Deng, R. Zhu, and X. Zhao (2005), Quantifying grain size distribution of pedogenic magnetic particles in Chinese loess and its significance for pedogenesis, *J. Geophys. Res.*, *110*, B11102, doi:10.1029/2005JB003726.

Liu, Q. S., A. P. Roberts, J. Torrent, C.-S. Horng, and J. C. Larrasoaña (2007), What do the HIRM and S-ratio really measure in environmental magnetism?, *Geochem. Geophys. Geosyst.*, *8*, Q09011, doi:10.1029/2007GC001717.

Liu, Q. S., V. Barrón, J. Torrent, S. G. Eeckhout, and C. Deng (2008), Magnetism of intermediate hydromaghemite in the transformation of 2-line ferrihydrite into hematite and its paleoenvironmental implications, *J. Geophys. Res.*, *113*, B01103, doi:10.1029/2007JB005207.

Maher, B. A. (1988), Magnetic properties of some synthetic sub-micron magnetites, *Geophys. J.*, *94*(1), 83–96, doi:10.1111/j.1365-246X.1988.tb03429.x.

McEnroe, S. A., K. Fabian, P. Robinson, C. Gaina, and L. L. Brown (2009), Crustal magnetism, lamellar magnetism and rocks that remember, *Elements*, *5*, 241–246, doi:10.2113/gselements.5.4.241.

Michel, F. M., V. Barrón, J. Torrent, M. P. Morales, C. J. Serna, J.-F. Boily, Q. Liu, A. Ambrosini, A. C. Cismasu, and G. E. Brown (2010), Ordered ferromagnetic form of ferrihydrite reveals links among structure, composition, and magnetism, *Proc. Natl. Acad. Sci. U. S. A.*, *107*, 2787–2792, doi:10.1073/pnas.0910170107.

Moriya, T. (1960), Anisotropic superexchange interaction and weak ferromagnetism, *Phys. Rev.*, *120*(1), 91–98, doi:10.1103/PhysRev.120.91.

Morrish, A. (1994), *Canted Antiferromagnetism: Hematite*, World Sci., Singapore.

Mørup, S., D. E. Madsen, C. Frandsen, C. R. H. Bahl, and M. F. Hansen (2007), Experimental and theoretical studies of nanoparticles of antiferromagnetic materials, *J. Phys. Condens. Matter.*, *19*, 213202, doi:10.1088/0953-8984/19/21/213202.

Moskowitz, B. M. (1981), Methods for estimating Curie temperatures of titanomaghemites from experimental Js-T data, *Earth Planet. Sci. Lett.*, *53*, 84–88, doi:10.1016/0012-821X(81)90028-5.

Nørnberg, P., U. Schwertmann, H. Stanjek, T. Andersen, and H. P. Gunnlaugsson (2004), Mineralogy of a burned soil compared with four anomalously red Quaternary deposits in Denmark, *Clay Miner.*, *39*(1), 85–98, doi:10.1180/000985543910122.

Nørnberg, P., A. L. Vendelboe, H. P. Gunnlaugsson, J. P. Merrison, K. Finster, and S. K. Jensen (2009), Comparison of the mineralogical effects of an experimental forest fire on a goethite/ferrihydrite soil with a topsoil that contains hematite, maghemite and goethite, *Clay Miner.*, *44*(2), 239–247, doi:10.1180/claymin.2009.044.2.239.

Özdemir, Ö., and D. J. Dunlop (2002), Thermoremanence and stable memory of single-domain hematites, *Geophys. Res. Lett.*, *29*(18), 1877, doi:10.1029/2002GL015597.

Özdemir, Ö., and D. J. Dunlop (2005), Thermoremanent magnetization of multidomain hematite, *J. Geophys. Res.*, *110*, B09104, doi:10.1029/2005JB003820.

Özdemir, Ö., and D. J. Dunlop (2006), Magnetic memory and coupling between spin-canted and defect magnetism in hematite, *J. Geophys. Res.*, *111*, B12S03, doi:10.1029/2006JB004555.

Özdemir, Ö., D. J. Dunlop, and T. S. Berquo (2008), Morin transition in hematite: Size dependence and thermal hysteresis, *Geochem. Geophys. Geosyst.*, *9*, Q10Z01, doi:10.1029/2008GC002110.

Porath, H. (1968), Stress induced magnetic anisotropy in natural single crystals of hematite, *Philos. Mag.*, *17*(147), 603–608, doi:10.1080/14786436808217746.

Rendón, J. L., J. Cornejo, P. de Arambarri, and C. J. Serna (1983), Pore structure of thermally treated goethite (α-FeOOH), *J. Colloid Interface Sci.*, *92*(2), 508–516, doi:10.1016/0021-9797(83)90172-8.

Roberts, A. P., Y. Cui, and K. L. Verosub (1995), Wasp-waisted hysteresis loops: Mineral magnetic characteristics and discrimination of components in mixed magnetic systems, *J. Geophys. Res.*, *100*(B9), 17,909–17,924, doi:10.1029/95JB00672.

Schulze, D. (1984), The influence of aluminium on iron oxides. VIII. Unit cell dimensions of Al substituted goethites and estimation of A1 from them, *Clays Clay Miner.*, *32*(1), 36–44, doi:10.1346/CCMN.1984.0320105.

Schwertmann, U., and R. M. Cornell (2000), *Iron Oxides in the Laboratory Preparation and Characterization*, VCH Weinheim, New York.

Schwertmann, U., R. Fitzpatrick, R. Taylor, and D. Lewis (1979), The influence of aluminum on iron oxides, Part II: Preparation and properties of Al substituted hematites, *Clays Clay Miner.*, *27*, 105–112, doi:10.1346/CCMN.1979.0270205.

Smith, R., and M. Fuller (1967), Alpha-hematite: Stable remanence and memory, *Science*, *156*, 1130–1133, doi:10.1126/science.156.3778.1130.

Spencer, E., and F. G. Percival (1952), The structure and origin of the banded hematite jaspers of Singhbhum, India, *Econ. Geol.*, *47*(4), 365–383, doi:10.2113/gsecongeo.47.4.365.

Stanjek, H., and U. Schwertmann (1992), The influence of aluminum on iron oxides, Part XVI: Hydroxyl and aluminum substitution in synthetic hematites, *Clays Clay Miner.*, *40*, 347–354, doi:10.1346/CCMN.1992.0400316.

Tauxe, L. (2010), *Essentials of Paleomagnetism*, Univ. of Calif. Press, Berkeley.

Taylor, R., and U. Schwertmann (1980), The influence of aluminum on iron oxides, VII. Substitution of A1 for Fe in synthetic lepidocrocite, *Clays Clay Miner.*, *28*(4), 267–271, doi:10.1346/CCMN.1980.0280404.

Torrent, J., V. Barrón, and U. Schwertmann (1990), Phosphate adsorption and desorption by goethites differing in crystal morphology, *Soil Sci. Soc. Am. J.*, *54*(4), 1007–1012, doi:10.2136/sssaj1990.03615995005400040012x.

Vandenberghe, R., C. Barrero, G. M. da Costa, E. van San, and E. de Grave (2000), Mössbauer characterization of iron oxides and (oxy) hydroxides: The present state of the art, *Hyperfine Interact.*, *126*(1–4), 247–259, doi:10.1023/A:1012603603203.

van der Zee, C., D. R. Roberts, D. G. Rancourt, and C. P. Slomp (2003), Nanogoethite is the dominant reactive oxyhydroxide phase in lake and marine sediments, *Geology*, *31*(11), 993–996, doi:10.1130/G19924.1.

Walker, T. R. (1967a), Formation of red beds in modern and ancient deserts, *Geol. Soc. Am. Bull.*, *78*(3), 353–368, doi:10.1130/0016-7606(1967)78[353:FORBIM]2.0.CO;2.

Walker, T. R. (1967b), Color of recent sediments in tropical Mexico: A contribution to the origin of red beds, *Geol. Soc. Am. Bull.*, *78*(7), 917–920, doi:10.1130/0016-7606(1967)78[917:CORSIT]2.0.CO;2.

Walker, T. R., E. E. Larson, and R. P. Hoblitt (1981), Nature and origin of hematite in the Moenkopi Formation (Triassic), Colorado Plateau: A contribution to the origin of magnetism in red beds, *J. Geophys. Res.*, *86*(B1), 317–333, doi:10.1029/JB086iB01p00317.

Wells, M. (1989), Formation of corundum and aluminous hematite by thermal dehydroxylation of aluminous goethite, *Clay Miner.*, *24*(3), 513–530, doi:10.1180/claymin.1989.024.3.05.

Wells, M. A., R. W. Fitzpatrick, R. J. Gilkes, and J. Dobson (1999), Magnetic properties of metal-substituted haematite, *Geophys. J. Int.*, *138*(2), 571–580, doi:10.1046/j.1365-246X.1999.00840.x.

V. Barrón and J. Torrent, Departamento de Agronomía, Universidad de Córdoba, Edificio C4, Campus de Rabanales, ES-14071 Córdoba, Spain.

Z. Jiang and Q. Liu, State Key Laboratory of Lithospheric Evolution, Institute of Geology and Geophysics, Chinese Academy of Sciences, Beijing 100029, China. (liux0272@yahoo.com)

Y. Yu, Department of Geology and Earth Environmental Sciences, Chungnam National University, Daejeon 305-764, South Korea.